Appl. Phys. A 81, 1519–1525 (2005)
DOI: 10.1007/s00339-005-3389-8

Applied Physics A
Materials Science & Processing

J. BÜRKI
C.A. STAFFORD✉

On the stability and structural dynamics of metal nanowires

Department of Physics, University of Arizona, 1118 E. 4th Street, Tucson, AZ 85721, USA

Received: 22 April 2005/Accepted: 23 August 2005
Published online: 27 September 2005 •

ABSTRACT This article presents a brief review of the nanoscale free-electron model, which provides a continuum description of metal nanostructures. It is argued that surface and quantum-size effects are the two dominant factors in the energetics of metal nanowires, and that much of the phenomenology of nanowire stability and structural dynamics can be understood based on the interplay of these two competing factors. A linear stability analysis reveals that metal nanocylinders with certain magic conductance values $G =$ 1, 3, 6, 12, 17, 23, 34, 42, 51, 67, 78, 96, ... times the conductance quantum are exceptionally stable. A nonlinear dynamical simulation of nanowire structural evolution reveals a universal equilibrium shape consisting of a magic cylinder suspended between unduloidal contacts. The lifetimes of these metastable structures are also computed.

PACS 68.65.La; 47.20.Dr; 61.46.+w; 68.35.Ja

1 Introduction

A macroscopic analysis of the mechanical properties of thin metal wires suggests that it might be difficult to fabricate wires thinner than a few thousand atoms in cross section: consider a cylindrical wire of radius R and length L. The maximum stress that the wire can sustain before the onset of plastic flow is σ_Y, the yield strength. On the other hand, the surface-induced stress in a thin wire is σ_s/R, where σ_s is the surface tension. If $\sigma_s/R > \sigma_Y$, one would expect the wire to undergo plastic flow and, if $L > 2\pi R$, to break up under surface tension, as in the Rayleigh instability of a column of fluid [1]. This estimate gives a minimum radius for solidity, $R_{min} = \sigma_s/\sigma_Y$. The parameters for several simple metals are given in Table 1. Plateau realized as early as 1873 that this surface-tension-driven instability of a cylinder is unavoidable if cohesion is due solely to classical pairwise interactions between atoms [2].

A great deal of experimental evidence has accumulated over the past decade, however, indicating that metal wires considerably thinner than the above estimate can be fabricated by a number of different techniques [6–20]. Even wires with lengths significantly exceeding their circumference were found to be remarkably stable [8–10, 17–19], indicating that some new mechanism must intervene to prevent their breakup.

Metal	σ_Y (MPa)	σ_s (N/m)	γ_s (pN)	σ_s/σ_Y (nm)	G_{min} (G_0)
Cu	210	1.5	190	7.1	2300
Ag	140	1.0	154	7.4	1900
Au	100	1.3	257	13	5600
Li	15	0.44	99	29	26000
Na	10	0.22	39	22	10000

TABLE 1 The yield strength σ_Y [3], surface tension σ_s [4], and curvature energy γ_s [5] of various monovalent metals. For a wire of radius $R < \sigma_s/\sigma_Y$, the stress due to surface tension exceeds σ_Y, signalling a breakdown of macroscopic elasticity theory. The electrical conductance G_{min} of a ballistic wire of radius $R_{min} = \sigma_s/\sigma_Y$ is shown in the *rightmost column* in units of the conductance quantum $G_0 = 2e^2/h$. Note that G/G_0 is approximately equal to the number of atoms that fit within the cross section for monovalent metals

A clue to the resolution of this problem was provided by the observation of electron-shell structure in conductance histograms of alkali-metal point contacts [11, 14–16]. Like the surface tension, quantum-size effects arising from the confinement of the conduction electrons within the cross section of the wire become increasingly important as the wire is scaled down to atomic dimensions. In fact, a linear stability analysis [21, 22] of ultra-thin metal wires within the free-electron model found that the Rayleigh instability can be completely suppressed in the vicinity of certain magic radii.

In this article, we argue that surface and quantum-size effects are the two dominant factors in the energetics of metal nanowires, that is, metal wires with $R < R_{min}$. We show that much of the phenomenology of nanowire stability and structural dynamics can be understood based on the interplay of these two competing factors.

This article is organized as follows: in Sect. 2 we describe our continuum structural model for metal nanowires. A linear stability analysis of metal nanowires is presented in Sect. 3. Section 4 describes the structural evolution of a metal nanowire from a random initial configuration to a universal equilibrium shape. The thermally activated decay of metal nanowires is discussed in Sect. 5. Some concluding remarks are given in Sect. 6.

✉ Fax: 001 520 621 472 1, E-mail: stafford@physics.arizona.edu

2 The nanoscale free-electron model

Guided by the importance of conduction electrons in the cohesion of metals, and by the success of the jellium model in describing metal clusters [23], the nanoscale free-electron model (NFEM) [24] replaces the metal ions by a uniform, positively charged background that provides a confinement potential for the electrons. The electron motion is free along the wire, and confined in the transverse directions. Due to the excellent screening [25, 26] in metal wires with $G > G_0$, electron–electron interactions can in most cases be neglected. The surface properties of various metals can be fitted by using appropriate surface boundary conditions [27, 28].

The NFEM is especially suitable for alkali metals, but is also adequate to describe shell effects due to the conduction-band *s* electrons in other monovalent metals, such as gold. The experimental observation of a crossover from atomic-shell to electron-shell effects with decreasing radius in both metal clusters [29] and nanowires [15, 16] justifies *a posteriori* the use of the NFEM in the latter regime.

A nanowire connecting two macroscopic electrodes is an open quantum system, for which the Schrödinger equation is most naturally formulated as a scattering problem. Transport properties can be obtained from the scattering matrix using Landauer-type formulas [24, 30, 31], while cohesive properties require the computation of the grand canonical potential of the electrons. The latter can also be expressed in terms of the scattering matrix [24], or calculated semiclassically [32] in terms of geometrical quantities and a sum over classical periodic orbits, as presented in Sect. 2.1.

Motivated by the argument presented in Table 1, the ionic degrees of freedom in the wire are modeled as an incompressible, irrotational fluid [22, 33]. In the Born–Oppenheimer approximation, the electronic free energy serves as the potential energy for the ions. The ionic dynamics may then be modeled via a surface self-diffusion equation [33], as presented in Sect. 2.3.1 or, taking thermal fluctuations into account, via a classical Ginzburg–Landau stochastic field theory [34], as presented in Sect. 2.3.2.

2.1 *Electronic energy functional*

Restricting ourselves to axisymmetric structures, the grand canonical potential for the electrons Ω_e becomes a functional of the radius $R(z)$ of the wire. Using the Weyl expansion [35], Ω_e can be expressed in terms of geometrical quantities such as the volume $\mathcal{V}$, surface area $\mathcal{S}$, and integrated mean curvature $\mathcal{C}$ of the wire's surface, plus an electron-shell correction,

$$\Omega_\mathrm{e}\big[R(z),T\big] = -\omega\mathcal{V} + \sigma_\mathrm{s}\mathcal{S} - \gamma_\mathrm{s}\mathcal{C} + \int_0^L \mathrm{d}z\, V_\mathrm{shell}\,, \tag{1}$$

where $-\omega$ is the bulk value per unit volume, σ_s is the surface tension, γ_s is a curvature-energy density, and $V_\mathrm{shell}\big(R(z),T\big)$ is a mesoscopic electron-shell potential, shown in Fig. 1. The parameters σ_s and γ_s, tabulated for various metals in Table 1, depend on the details of the interaction-dependent surface confinement potential [27, 28, 32], but can be taken as phenomenological material-dependent parameters (along with ω) in our model. The leading-order electron-shell correction is, however, independent of the Coulomb interaction [25, 26, 32], and therefore insensitive to the details of the confinement potential.

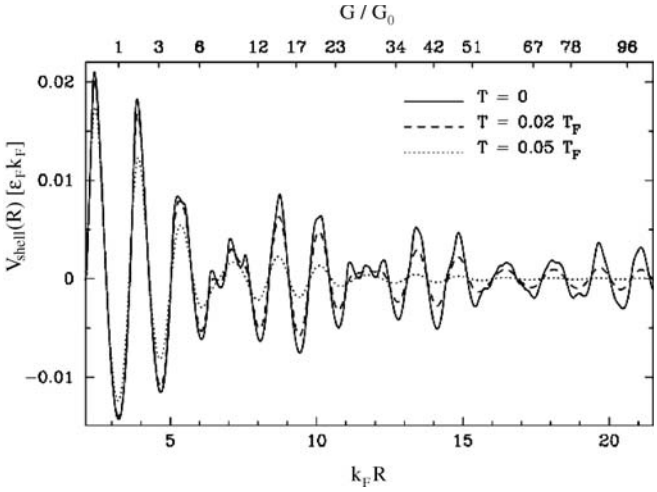

FIGURE 1 Electron-shell potential $V_\mathrm{shell}(R,T)$ at zero and two finite temperatures, which correspond respectively to 1000 K and 2500 K for Na. The electrical conductance values of the magic cylindrical wires are indicated on the *upper axis*

The geometrical quantities $\mathcal{S} = \int_0^L \mathrm{d}z\,\partial\mathcal{S}$ and $\mathcal{C} = \int_0^L \mathrm{d}z\,\partial\mathcal{C}$ are given by

$$\partial\mathcal{S}\big[R(z)\big] = 2\pi R(z)\sqrt{1+(\partial_z R)^2} \tag{2}$$

and

$$\partial\mathcal{C}\big[R(z)\big] = \pi\left(1 - \frac{R\partial_z^2 R}{1+(\partial_z R)^2}\right), \tag{3}$$

where $\partial_z = \partial/\partial z$.

Approximating the confining potential by a hard wall at the surface of the wire, the electron-shell potential V_shell can be expressed in terms of a Gutzwiller-type trace formula [33]

$$V_\mathrm{shell}(R,T) = \frac{2\varepsilon_\mathrm{F}}{\pi}\sum_{w=1}^{\infty}\sum_{v=2w}^{\infty} a_{vw}(T)\frac{f_{vw}\cos\theta_{vw}}{v^2 L_{vw}}\,, \tag{4}$$

where the sum includes all classical periodic orbits (v, w) in a disk billiard [35], characterized by their number of vertices v and winding number w, $L_{vw} = 2vR\sin(\pi w/v)$ is the length of orbit (v, w), and $\theta_{vw} = k_\mathrm{F}L_{vw} - 3v\pi/2$. The factor $f_{vw} = 1$ for $v = 2w$, 2 otherwise, accounts for the invariance under time-reversal symmetry of some orbits, and $a_{vw}(T) = \tau_{vw}/\sinh\tau_{vw}$ ($\tau_{vw} = \pi k_\mathrm{F}L_{vw}T/2T_\mathrm{F}$) is a temperature-dependent damping factor.

$V_\mathrm{shell}(R)$ exhibits deep minima as a function of R (see Fig. 1), suggesting that some radii are strongly favored, which is confirmed by the stability analysis of Sect. 3. Note that room temperature is small compared to the Fermi temperature $T_\mathrm{F} = \varepsilon_\mathrm{F}/k_\mathrm{B}$ (in particular, $T/T_\mathrm{F} = 0.008$ at $T = 300$ K for Na), so that the finite-temperature electron-shell potential is essentially indistinguishable from its zero-temperature limit at experimental temperatures.

2.2 *Ionic energetics*

In the Born–Oppenheimer approximation, the electronic energy (1) acts as a potential energy for the ionic background. The wire can exchange atoms with the macroscopic contacts via surface self-diffusion, so the grand canonical ensemble has to be used for the ionic background as well, leading to an ionic grand canonical potential

$$\Omega_{\rm a} = \Omega_{\rm e} - \mu_{\rm a}\mathcal{N}_{\rm a}\,, \tag{5}$$

where $\mathcal{N}_{\rm a} = \mathcal{V}/\mathcal{V}_{\rm a}$ is the number of positive ions in the wire ($\mathcal{V}_{\rm a} = 3\pi^2/k_{\rm F}^3$ is the volume of an atom) and $\mu_{\rm a}$ is the chemical potential for a surface atom in the wire. Using Eqs. (1)–(3), the ionic free energy (5) becomes

$$\Omega_{\rm a} = \int {\rm d}z \Big[2\pi\sigma_{\rm s} R(z,t)\sqrt{1+(\partial_z R)^2} - \pi\gamma_{\rm s} + V_{\rm shell}(R,T) \Big] - (\omega + \mu_{\rm a}/\mathcal{V}_{\rm a})\mathcal{V}\,, \tag{6}$$

where only the leading-order term in the curvature energy is included. The chemical potential $\mu_{\rm a}$ is obtained by calculating the change in the energy (1) with the addition of an atom at point z_0, $\mu_{\rm a}(z_0) \equiv c\delta\Omega_{\rm e}[R(z)]/\delta R(z_0) = \Omega_{\rm e}\big[R(z) + c\delta(z-z_0), T\big] - \Omega_{\rm e}\big[R(z), T\big]$, where $c = \mathcal{V}_{\rm a}/2\pi R(z)$ is chosen so that the volume of an atom is added:

$$\mu_{\rm a}(z) = -\omega\mathcal{V}_{\rm a} + \frac{\mathcal{V}_{\rm a}}{2\pi R}\left(\frac{2\sigma_{\rm s}\partial\mathcal{C}[R(z)]}{\sqrt{1+(\partial_z R)^2}} + \frac{\partial V_{\rm shell}}{\partial R} \right). \tag{7}$$

2.3 *Structural dynamics*

2.3.1 Surface self-diffusion. Since a large fraction of the atoms in a nanowire are on the surface, surface self-diffusion is the dominant mechanism of ionic motion [33]. The dynamics derive from ionic mass conservation:

$$\frac{\pi}{\mathcal{V}_{\rm a}}\frac{\partial R^2(z,t)}{\partial t} + \frac{\partial}{\partial z}\big[2\pi R(z,t) J_z(z,t)\big] = 0\,, \tag{8}$$

where the z component of the surface current density is given by Fick's law:

$$J_z = -\frac{\varrho_{\rm S} D_{\rm S}}{k_{\rm B}T}\frac{1}{\sqrt{1+(\partial_z R)^2}}\frac{\partial\mu_{\rm a}}{\partial z}\,. \tag{9}$$

Here, $\varrho_{\rm S}$ and $D_{\rm S}$ are the surface density of ions and the surface self-diffusion coefficient, respectively. The precise value of $D_{\rm S}$ for most metals is not known, but it can be removed from the evolution equation by rescaling time to the dimensionless variable $\tau = (\varrho_{\rm S} D_{\rm S} T_{\rm F}/T)t$. For comparison with experimental time scales, one can estimate that for quasi-one-dimensional diffusion $D_{\rm S} \approx \nu_{\rm D} a^2 \exp(-E_{\rm S}/k_{\rm B}T)$, where $\nu_{\rm D}$ is the Debye frequency, a is the lattice spacing, and $E_{\rm S}$ is an activation energy comparable to the energy of a single bond in the solid. Our nonlinear dynamical model, Eqs. (7)–(9), differs from previous studies of axisymmetric surface self-diffusion [36–38] by the inclusion of electron-shell effects (last term of Eq. (7)), which fundamentally alters the dynamics.

2.3.2 Thermal fluctuations. The diffusive dynamics of the previous subsection describe relaxation toward structures of lower free energy. Once an equilibrium configuration (i.e. a local minimum of the free energy) is attained, however, fluctuations about this configuration will dominate the dynamics, limiting the dwell time of the system in this local minimum. As shown in Sect. 4, the equilibrium configurations consist of stable cylindrical nanowires in diffusive equilibrium with unduloid-like contacts [33, 39]. We therefore study fluctuations of the form

$$R(z,t) \equiv R_0 + \varphi(z,t)\,, \tag{10}$$

where R_0 is the radius of a stable cylinder of length L.

The energy (6) can be expanded as a series in φ. For the magic cylinders, corresponding to minima of $V_{\rm shell}(R_0)$ (cf. Fig. 1), the chemical potential for the exchange of atoms between the wire and the contacts reduces to

$$\frac{\mu_{\rm a}}{\mathcal{V}_{\rm a}} = \frac{\sigma_{\rm s}}{R_0} - \omega\,. \tag{11}$$

Keeping only the leading-order terms in $\partial_z\varphi$, one obtains $\Omega_{\rm a} = \Omega_{\rm a}(R_0) + \mathcal{H}[\varphi]$, where $\Omega_{\rm a}(R_0)$ is the energy of an unperturbed cylinder of radius R_0 and

$$\mathcal{H}[\varphi] = \int_0^L {\rm d}z \left[\frac{\kappa}{2}(\partial_z\varphi)^2 + V(\varphi) \right]. \tag{12}$$

Here, $\kappa = 2\pi\sigma_{\rm s}R_0$ and

$$V(\varphi) \equiv V_{\rm shell}(R_0+\varphi) - V_{\rm shell}(R_0) - \frac{\pi\sigma_{\rm s}}{R_0}\varphi^2\,. \tag{13}$$

The problem of stability of nanowires against thermal fluctuations can be studied as a one-dimensional Ginzburg–Landau scalar field theory, perturbed by weak spatiotemporal noise, in a domain of finite extent (see Ref. [34] and references therein): the fluctuations of the nanowire radius φ are treated as a classical field on a one-dimensional spatial domain $[0, L]$. Its dynamics are governed by the stochastic Ginzburg–Landau equation

$$\frac{\partial\varphi(z,t)}{\partial t} = \kappa\frac{\partial^2\varphi}{\partial z^2} - \frac{\partial V}{\partial\varphi} + (2T)^{1/2}\xi(z,t)\,, \tag{14}$$

where $\xi(z,t)$ is unit-strength spatiotemporal white noise, satisfying $\langle\xi(z_1,t_1)\xi(z_2,t_2)\rangle = \delta(z_1-z_2)\delta(t_1-t_2)$. In Eq. (14), time is measured in units of a microscopic time scale describing the short-wavelength cutoff of the surface dynamics [22], which is given to within a factor of order unity by the inverse Debye frequency $\nu_{\rm D}^{-1}$. The zero-noise dynamics is 'gradient', that is, at zero temperature $\dot\varphi = -\delta\mathcal{H}/\delta\varphi$, where $\mathcal{H}[\varphi]$ is given by Eq. (12). Equation (14) represents a considerable simplification compared to the volume-conserving dynamics of Eq. (8) (which involves derivatives up to $\partial_z^4 R$), and makes possible an analytical treatment of thermal fluctuations.

3 Linear stability of cylinders

The linear stability of a structure is determined by studying the change of energy induced by a small perturbation: if any one perturbation decreases the energy, the structure is unstable, while it is stable if all perturbations increase the energy.

The most general perturbation of a cylinder of radius R_0 and length L is

$$R(z,\varphi) = R_0 + \lambda \sum_m \sum_q b_m(q) \mathrm{e}^{\mathrm{i}(qz+m\varphi)} \,, \tag{15}$$

where $b_m(q) = b_{-m}(-q)^*$. For simplicity, we impose periodic boundary conditions, so that q is an integer multiple of $2\pi/L$. Since the total number of atoms in the system is unchanged by the perturbation, $b_0(0)$ is related to the other coefficients by volume conservation:

$$b_0(0) = -\frac{\lambda}{R_0} \sum_m \sum_{q>0} |b_m(q)|^2 + \mathcal{O}\left(\lambda^2\right) \,, \tag{16}$$

and may be eliminated. Other constraints [28] may be utilized to account for confinement potentials more general [27] than the hard walls considered in the present article, but do not lead to a qualitative change in the stability analysis.

The energy change (per unit length) under such a perturbation is found to be

$$\frac{\Delta\Omega_\mathrm{e}}{L} = \lambda^2 \sum_m \sum_{q>0} \alpha_m(q;\, R_0, T) |b_m(q)|^2 + \mathcal{O}\left(\lambda^3\right) \,, \tag{17}$$

where the mode stiffness $\alpha_m(q)$ is given by

$$\begin{aligned}\alpha_m(q;\, R, T) =& (m^2-1)\frac{2\pi\sigma_\mathrm{s}}{R} + 2\pi(\sigma_\mathrm{s} R - \gamma_\mathrm{s}) q^2 \\ &+ \delta\alpha_m(q;\, R, T) \,,\end{aligned} \tag{18}$$

and $\delta\alpha_m$ is a mesoscopic electron-shell correction.

Neglecting for the moment the mesoscopic correction $\delta\alpha_m(q)$, we find that the perturbation can lead to an instability only for $m = 0$ and $qR_0 < \left(1 - \gamma_\mathrm{s}/\sigma_\mathrm{s} R_0\right)^{-1/2} \approx 1$, which is the criterion for the classical Rayleigh instability [1]. Note that $\sigma_\mathrm{s} R_0 > \gamma_\mathrm{s}$ for all physically meaningful radii (cf. Table 1). Any perturbation breaking axial symmetry is classically unfavorable, and we will therefore consider only axisymmetric perturbations ($m = 0$) in the rest of this paper.

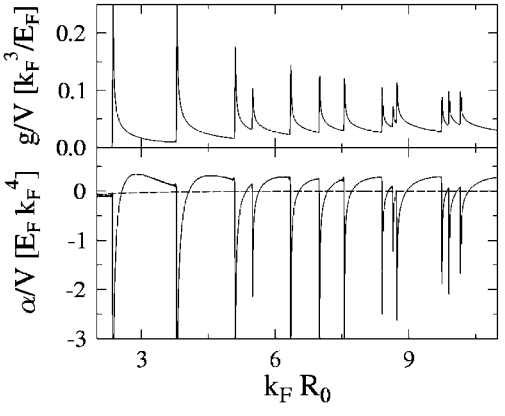

FIGURE 2 Density of states at the Fermi energy g (*top*) and mode stiffness for axisymmetric deformations $\alpha \equiv \alpha_0(q)$ (*bottom*), normalized by the volume $\mathcal{V}$ of the wire. The perturbation wavevector is given by $qR_0 = 1$, so that the surface contribution (*dashed curve*) to α is nearly zero

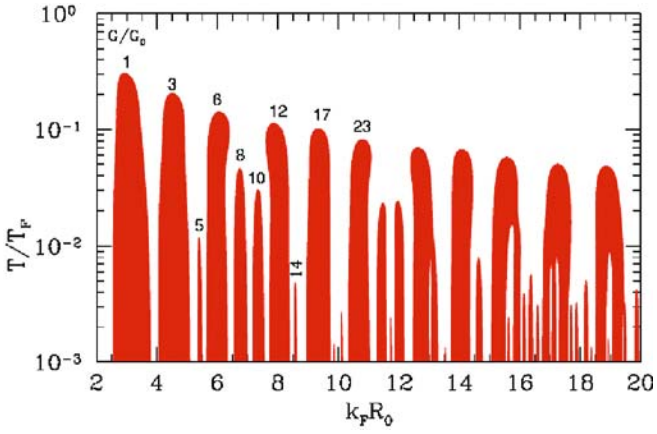

FIGURE 3 Stability diagram for cylindrical metal nanowires. *Dark areas* indicate stability with respect to small perturbations, $A(R_0, T) > 0$. The quantized conductance values of some of the stable wires are indicated

Using semiclassical perturbation theory, the electron-shell correction to the mode stiffness for axisymmetric deformations was found to be independent of q [21, 22],

$$\delta\alpha_0(R, T) = \left(\frac{\partial^2}{\partial R^2} - \frac{1}{R}\frac{\partial}{\partial R}\right) V_\mathrm{shell}(R, T) \,. \tag{19}$$

This turns out to be true only in the semiclassical approximation: a fully quantum-mechanical stability analysis [40] reveals that long wires undergo a Peierls-type instability at $q = 2k_\mathrm{F}^{(\nu)}$, where $k_\mathrm{F}^{(\nu)}$ is the Fermi wavevector for subband ν. However, the semiclassical results are found to provide a good approximation as long as the temperature is not too low, and the wires are not too long [40]. The total mode stiffness $\alpha_0(q = 1/R_0)$ in the semiclassical approximation is shown in Fig. 2, together with the density of states $g(\varepsilon_\mathrm{F})$. The perturbation wavevector was chosen so that the surface contribution to α_0 (dashed curve) is nearly zero. Figure 2 shows that near the thresholds to open new conducting channels, where the density of states is large, the wire is very unstable ($\alpha_0 < 0$). However, in between the subband thresholds, the shell correction stabilizes the wire ($\alpha_0 > 0$).

According to Eqs. (18) and (19), the most unstable mode is $m = 0, q = 0$. The stability of the wire is thus determined by the sign of the stability coefficient $A(R_0, T) \equiv \alpha_0 (q = 0;\, R_0, T)$,

$$A(R, T) = -\frac{2\pi\sigma_\mathrm{s}}{R} + \left(\frac{\partial^2}{\partial R^2} - \frac{1}{R}\frac{\partial}{\partial R}\right) V_\mathrm{shell}(R, T) \,. \tag{20}$$

For $A > 0$, the wire is stable with respect to all small perturbations, while the wire is unstable for $A < 0$. The stability diagram so determined is shown in Fig. 3. Competition between surface tension and electron-shell effects leads to a complex landscape of stable fingers and arches extending up to very high temperatures: cylindrical wires whose electrical conductance is a magic number 1, 3, 6, 12, 17, 23, ... times the

conductance quantum are predicted to be stable with respect to small perturbations up to temperatures well above the bulk melting temperature $T_M \approx 0.01 T_F$. This finding suggests that metal nanowires are remarkably robust structures. Indeed, the principal stable zones shown in Fig. 3 were found [26] to persist up to bias voltages $eV \geq 0.1\varepsilon_F$, implying that these wires can support current densities greater than 10^{10} A/cm^2, which would vaporize a macroscopic wire. (See Sect. 5 for a discussion of nanowire lifetime as a function of temperature.) In Fig. 3, the values [32] $\sigma_s = \varepsilon_F k_F^2/80\pi$ and $\gamma_s = 4\varepsilon_F k_F/45\pi^2$, appropriate for alkali metals [22], were used. For larger values of σ_s (e.g. for noble metals), the maximum temperatures (in units of T_F) of the stable fingers are reduced somewhat, but the stability diagram is qualitatively the same.

The fact, illustrated in Fig. 3, that electron-shell effects can overcome the surface-tension-driven instability of a cylinder is rather remarkable. The surface contribution to Ω_e is $\mathcal{O}(k_F R_0)$, while the electron-shell contribution (4) is $\mathcal{O}(k_F R_0)^{-1}$. For a typical radius $k_F R_0 = 10$, the shell correction to the energy is thus two orders of magnitude smaller than the surface energy! Stability is not determined by the energy directly, however, but rather by the convexity (or lack thereof) of the energy functional, which involves the second derivative with respect to R_0 (cf. Eq. (20)). Because V_{shell} is a rapidly oscillating function of R_0, its second derivative actually has the same characteristic size as the surface contribution to the stability coefficient (first term on the right-hand side of Eq. (20)).

Cylinders are special in this respect, because the term $\mathcal{O}(\lambda)$ in Eq. (17) vanishes exactly by symmetry. For a more general shape (such as a wire with an elliptical cross section [28]) to be stable, the first variations of the surface energy and electron-shell energy, which do not have the same characteristic size, must cancel. This is only possible for small $k_F R_0$ and/or for small deviations from cylindrical symmetry. Thus, cylinders represent about 75% of the experimentally observable [41] (most stable) wires, while structures of lesser symmetry represent only about 25% of the total.

Further insight into the stability criterion $A(R_0, T) > 0$ is provided by the identity

$$\left.\frac{\partial \mu_{cyl}(R_0, T)}{\partial R_0}\right|_T = \frac{\mathcal{V}_a}{2\pi R_0} A(R_0, T)\,, \qquad (21)$$

where $\mu_{cyl}(R_0, T)$ is given by Eq. (7) with $R(z) = R_0$. The wire can lower its free energy via phase separation into thicker and thinner segments if and only if $\partial\mu_{cyl}/\partial R_0 < 0$. $A < 0$ therefore corresponds to an inhomogeneous phase [22], while $A > 0$ corresponds to a homogeneous phase. This is confirmed by dynamical simulation of weakly perturbed stable and unstable cylinders, the latter evolving into an inhomogeneous wire [33].

4 Evolution toward equilibrium

In this section, we use the diffusion equation (8) to study the equilibrium shapes of metal nanowires, as well as the approach to equilibrium. Figure 4 shows three stages of the typical evolution [33, 39] of an initially random (a) nanowire: after a relatively short time (b), the short-wavelength surface roughness is smoothed out, leaving a few cylindrical segments, connected by kinks; eventually, all kinks propagate outward and coalesce, yielding an equilibrium shape (c) consisting of a cylindrical wire suspended between two thicker contacts.

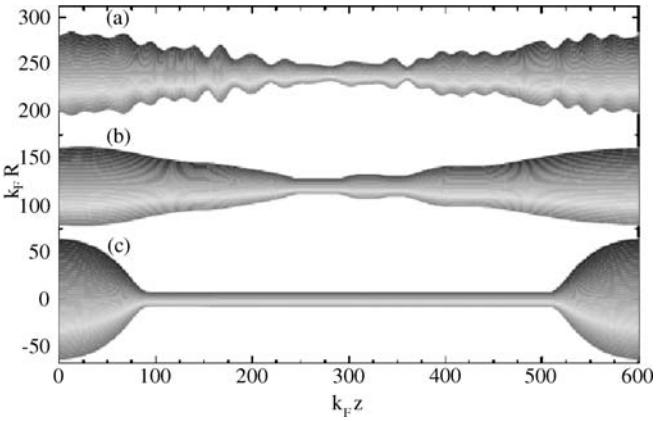

FIGURE 4 Equilibration of an initially random nanowire: (a) initial shape; (b) $\tau = 2 \times 10^4$; (c) $\tau = 3 \times 10^7$, equilibrium structure with $G = 12G_0$

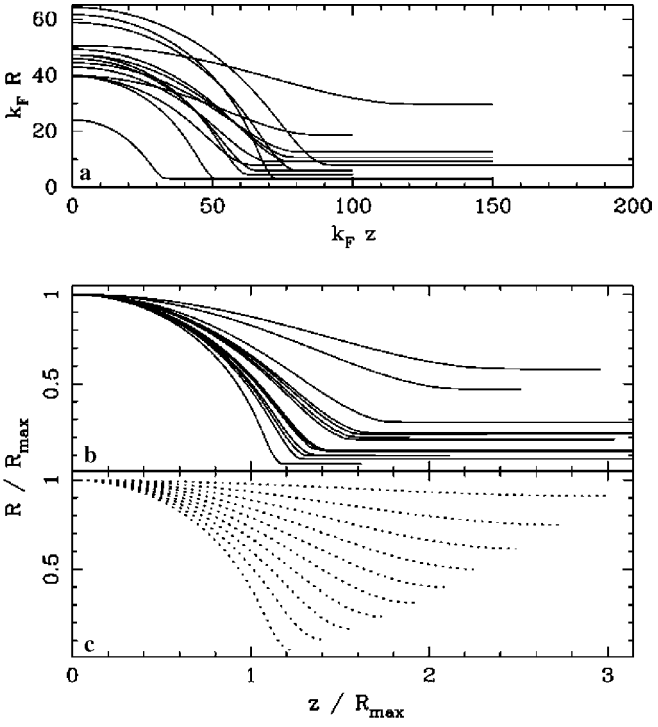

FIGURE 5 (**a**) Radius $R(z)$ of the equilibrium shapes for 14 simulations starting from random initial shapes; the equilibrium shapes being symmetric (although the initial shapes are not), we only show $R(z)$ for $z \in [0, L/2]$. (**b**) Same shapes rescaled by their maximum radius R_{max}. (**c**) Series of Delaunay unduloids of various curvatures

Several such simulations starting from various initial configurations, with conductances ranging from 1 to $200G_0$, and lengths $200 \leq k_F L \leq 600$, all evolved to equilibrium structures consisting of one of the stable cylinders found in Sect. 3, connecting two quasi-spherical contacts (see Fig. 5a). The shape of the contact is actually a close approximation to a Delaunay unduloid of revolution [38], which is a surface of constant mean curvature, and is an unstable steady state of the diffusion equation (8) without the shell-effect term. This is il-

lustrated in Fig. 5, comparing the equilibrium wires, rescaled (b) by their maximum radius $R_{\max}$ to a series of unduloids (c) of various mean curvatures. The curvature of the unduloid is determined solely by the ratio of the radius of the cylindrical part to $R_{\max}$, and not by the conductance of the wire or its length. In our case, the deep minima of the electron-shell potential, Fig. 1, pin the unduloid at its connection with the cylindrical part, thus stabilizing it. In fact, if one switches off the electron-shell potential in the simulations, the equilibrated wires break apart, as expected from the Rayleigh instability. The breaking is found to happen first at the junction between the cylinder and the lead, suggesting that it is the weak point of the equilibrium structure.

This suggests that the natural evolution of a nanowire, at a temperature sufficient for surface atoms to diffuse, is to form a cylinder, thus providing an explanation of the observation of long, almost perfect cylindrical Au nanowires in transmission electron microscope (TEM) experiments [8, 12, 13, 18]. The same type of simulation can be used to understand the thinning process observed in TEM experiments [19], where the wire diameter is seen to decrease step by step through the propagation of kinks along the wire.

5 Lifetimes of metastable cylinders

The equilibrium nanowire structures determined in the preceding sections are stable with respect to small perturbations, and represent local minima of the free-energy functional (6). However, large perturbations induced e.g. by thermal fluctuations can drive the nanowire out of such a minimum, leading to a finite lifetime of these metastable structures. In this section, we use the stochastic model [34] derived in Sect. 2.3.2 to study this process.

The statistical properties of the stochastically evolving field φ, Eq. (10), are described by equilibrium statistical mechanics. At nonzero temperature, thermal fluctuations can induce transitions between stable states (i.e. local minima) of the potential $V(\varphi)$, Eq. (13)). Such transitions occur via nucleation of a 'droplet' of one stable configuration in the background of the other, subsequently quickly spreading to fill the entire spatial domain. When the noise is weak, i.e. at low temperatures (compared to the barrier height), most fluctuations will not succeed in nucleating a new phase; it is far more likely for a small droplet to shrink and vanish.

A transition state must go 'uphill' in energy from each stable field configuration. Because of exponential suppression of fluctuations as their energy increases, there is at low temperature a preferred transition configuration (saddle) that lies between adjacent minima. These are the nucleation pathways. By time-reversal invariance, they are time-reversed zero-noise 'downhill' trajectories [42]. At low temperatures, the expected waiting time of the order parameter φ in a basin of attraction is an exponential random variable, as is typical of slow-rate processes. The activation rate is given in the $T \to 0$ limit by the Kramers formula

$$\Gamma \sim \Gamma_0 \exp(-\Delta E/T)\,. \tag{22}$$

Here, the activation barrier ΔE is the energy of the transition state minus that of the stable state, and Γ_0 is the rate prefactor. The quantities ΔE and Γ_0 depend on the details of the potential, on the length L, and on the choice of boundary conditions at the endpoints $z = 0$ and $z = L$. Based on the equilibrium structures found in Sect. 4, we employ Neumann boundary conditions, $0 = \partial_z \varphi(z, t)|_{z=0,L}$. These boundary conditions force nucleation to begin, preferentially, at the endpoints, consistent with experimental observations [19].

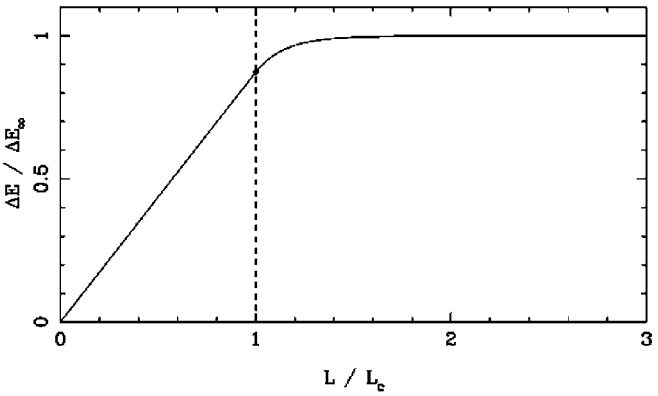

FIGURE 6 Escape barrier ΔE as a function of the wire length L. Here L_c is the critical length at which the transition state bifurcates

Equation (14) with the potential (13) cannot in general be solved analytically, but most minima of the potential $V(\varphi)$ can be locally approximated by a cubic potential

$$V^{(\pm)}(\varphi) = -\alpha\tilde{\varphi}_{\pm} + \frac{\beta}{3}\tilde{\varphi}_{\pm}^3\,, \tag{23}$$

where $\tilde{\varphi}_{\pm} = \sqrt{\alpha/\beta} \mp \varphi$ ($\alpha, \beta > 0$). The potential $V^{(-)}$ ($V^{(+)}$) biases fluctuations toward smaller (larger) radii.

Figure 6 shows the escape barrier ΔE as a function of the wire length [34]: below a critical length L_c, the transition state is a spatially constant field configuration, and the escape barrier grows linearly with the wire length L. However, at $L = L_c$ it bifurcates into a spatially varying instanton configuration with characteristic size $\sim L_c$, so that ΔE becomes length independent for $L \gg L_c$.

Our continuum dynamical model thus predicts that the lifetime τ of a metastable cylindrical nanowire of length greater than the critical length L_c saturates with an escape barrier given by $\Delta E_\infty = \lim_{L\to\infty} \Delta E$. In terms of the physical parameters defining the cubic potential (23), the critical length $L_c = (\pi/\sqrt{2})\kappa^{1/2}/(\alpha\beta)^{1/4}$ and $\Delta E_\infty = (12\sqrt{2}/5)\kappa^{1/2}\alpha^{5/4}/\beta^{3/4}$. The lifetimes $\tau = 1/\Gamma$ for several cylindrical sodium nanowires, calculated using the best cubic-polynomial fits to the potential (13), are tabulated in Table 2. Note that for a wire with $G/G_0 > 1$, the lifetime τ may not be the typical time before the wire breaks, but rather a switching time between two different metastable wires with different conductance values.

An important prediction given in Table 2 is that the lifetimes of the most stable nanowires, while they do exhibit significant variations from one conductance plateau to another, do not vary systematically as a function of radius; the activation barriers in Table 2 vary by only about 30% from one plateau to another, and the wire with a conductance of $96G_0$ has essentially the same lifetime as that with a conductance of $3G_0$. In this sense, the activation barrier is found to be universal: in any conductance interval, there are very short-lived

G (G_0)	L_c (Å)	ΔE_∞ (meV)	τ (s) 75 K	100 K	125 K
3	2.8	250	4×10^{5}	2	5×10^{-3}
6	4.3	200	7	3×10^{-3}	3×10^{-5}
17	5.0	260	7×10^{5}	3	8×10^{-3}
23	6.1	230	2×10^{3}	0.2	9×10^{-4}
42	7.2	250	2×10^{5}	1	10^{-3}
51	6.8	190	1	8×10^{-4}	10^{-4}
67	18.8	180	0.6	5×10^{-4}	7×10^{-6}
96	11.4	250	10^{5}	0.8	3×10^{-3}

TABLE 2 The lifetime τ (in seconds) for various cylindrical sodium nanowires at temperatures from 75 K to 125 K. Here G is the electrical conductance of the wire, L_c is the critical length above which the lifetime may be approximated by $\tau \approx \nu_D^{-1} \exp(\Delta E_\infty/T)$, and ΔE_∞ is the activation energy for an infinitely long wire. Note that wires shorter than L_c are predicted to have shorter lifetimes

wires (not shown in Table 2) with very small activation barriers, while the longest-lived wires have activation barriers of a universal size

$$\Delta E_\infty \simeq 0.6 \left(\frac{\hbar^2 \sigma_s}{m_e}\right)^{1/2}, \tag{24}$$

depending only on the surface tension of the material. Here, m_e is the conduction-band effective mass, which is comparable to the free-electron rest mass. A comparison of the lifetimes of sodium and gold nanowires [34] indicates that gold nanowires are much more stable, as expected from the larger value of the surface tension $\sigma_s(\mathrm{Au}) = 5.9\sigma_s(\mathrm{Na})$. This is consistent with the observation that gold nanowires in particular, and noble-metal nanowires in general, are much more stable than alkali-metal nanowires.

The fact that the typical activation energy (24) is independent of R_0 may be understood as follows: the instanton is a stationary state of Eq. (12); as such, the virial theorem implies that the bending energy $\langle \frac{1}{2}\kappa(\partial_z\varphi)^2\rangle$ is proportional to $\langle V(\varphi)\rangle$. Since $\kappa \sim \sigma_s R_0$ and $V \sim 1/R_0$, this implies that the characteristic size of the instanton $L_c \sim \sqrt{\sigma_s} R_0$ and $\Delta E_\infty \sim \sqrt{\sigma_s}$.

The lifetimes tabulated for sodium nanowires in Table 2 exhibit a rapid decrease in the temperature interval between 75 K and 125 K. This behavior can explain the observed temperature dependence of conductance histograms for sodium nanowires [11, 14, 16], which show clear peaks at conductances near the predicted values at temperatures below 100 K, but which were not reported at higher temperatures.

6 Discussion

The nanoscale free-electron model (NFEM) reviewed in the present article correctly describes surface and electronic quantum-size effects, which play an essential role in the stability and structural dynamics of metal nanowires; however, it does not address their discrete atomic structure. This continuum approach is thus complementary to atomistic simulations, such as tight-binding molecular dynamics [43], which correctly describe the effects of crystalline orientation, but include electronic quantum effects only to leading order.

It is hoped that the generic behavior of metal nanostructures elucidated by the NFEM can guide the exploration of more elaborate, material-specific models, in the same way that the free-electron model provides an important theoretical reference point from which to understand the complex properties of real bulk metals.

ACKNOWLEDGEMENTS This work was supported by NSF Grant No. 0312028. We thank Raymond Goldstein, Hermann Grabert, Frank Kassubek, Daniel Stein, Daniel Urban, and Chang-hua Zhang for their contributions to the work reviewed in this article.

REFERENCES

1 S. Chandrasekhar, *Hydrodynamic and Hydromagnetic Stability* (Dover, New York, 1981), pp. 515–574
2 J. Plateau, *Statique Expérimentale et Théorique des Liquides Soumis aux Seules Forces Moléculaires* (Gautier-Villars, Paris, 1873)
3 R.B. Ross, *Metallic Materials Specification Handbook* (Chapman and Hall, London, 1992)
4 W.R. Tyson, W.A. Miller, Surf. Sci. **62**, 267 (1977)
5 J.P. Perdew, Y. Wang, E. Engel, Phys. Rev. Lett. **66**, 508 (1991)
6 G. Rubio, N. Agraït, S. Vieira, Phys. Rev. Lett. **76**, 2302 (1996)
7 C. Untiedt, G. Rubio, S. Vieira, N. Agraït, Phys. Rev. B **56**(4), 2154 (1997)
8 Y. Kondo, K. Takayanagi, Phys. Rev. Lett. **79**, 3455 (1997)
9 H. Ohnishi, Y. Kondo, K. Takayanagi, Nature **395**, 780 (1998)
10 A.I. Yanson, G. Rubio Bollinger, H.E. van den Brom, N. Agraït, J.M. van Ruitenbeek, Nature **395**, 783 (1998)
11 A.I. Yanson, I.K. Yanson, J.M. van Ruitenbeek, Nature **400**, 144 (1999)
12 Y. Kondo, K. Takayanagi, Science **289**, 606 (2000)
13 V. Rodrigues, T. Fuhrer, D. Ugarte, Phys. Rev. Lett. **85**, 4124 (2000)
14 A.I. Yanson, I.K. Yanson, J.M. van Ruitenbeek, Phys. Rev. Lett. **84**, 5832 (2000)
15 A.I. Yanson, I.K. Yanson, J.M. van Ruitenbeek, Phys. Rev. Lett. **87**, 216805 (2001)
16 A.I. Yanson, J.M. van Ruitenbeek, I.K. Yanson, Low Temp. Phys. **27**, 807 (2001)
17 V. Rodrigues, J. Bettini, A.R. Rocha, L.G.C. Rega, D. Ugarte, Phys. Rev. B **65**, 153 402 (2002)
18 Y. Oshima, Y. Kondo, K. Takayanagi, J. Electron Microsc. **52**, 49 (2003)
19 Y. Oshima, A. Onga, K. Takayanagi, Phys. Rev. Lett. **91**, 205 503 (2003)
20 M. Díaz, J.L. Costa-Krämer, E. Medina, A. Hasmy, P.A. Serena, Nanotechnology **14**, 113 (2003)
21 F. Kassubek, C.A. Stafford, H. Grabert, R.E. Goldstein, Nonlinearity **14**, 167 (2001)
22 C.-H. Zhang, F. Kassubek, C.A. Stafford, Phys. Rev. B **68**, 165 414 (2003)
23 M. Brack, Rev. Mod. Phys. **65**, 677 (1993)
24 C.A. Stafford, D. Baeriswyl, J. Bürki, Phys. Rev. Lett. **79**, 2863 (1997)
25 F. Kassubek, C.A. Stafford, H. Grabert, Phys. Rev. B **59**, 7560 (1999)
26 C.-H. Zhang, J. Bürki, C.A. Stafford, Phys. Rev. B **71**, 235 404 (2005)
27 A. García-Martin, J.A. Torres, J.J. Sáenz, Phys. Rev. B **54**, 13 448 (1996)
28 D.F. Urban, J. Bürki, C.-H. Zhang, C.A. Stafford, H. Grabert, Phys. Rev. Lett. **93**, 186 403 (2004)
29 T.P. Martin, Phys. Rep. **273**, 199 (1996)
30 J. Bürki, C.A. Stafford, X. Zotos, D. Baeriswyl, Phys. Rev. B **60**, 5000 (1999)
31 J. Bürki, C.A. Stafford, Phys. Rev. Lett. **83**, 3342 (1999)
32 C.A. Stafford, F. Kassubek, J. Bürki, H. Grabert, Phys. Rev. Lett. **83**, 4836 (1999)
33 J. Bürki, R.E. Goldstein, C.A. Stafford, Phys. Rev. Lett. **91**, 254 501 (2003)
34 J. Bürki, C.A. Stafford, D.L. Stein, Phys. Rev. Lett. **95**, 090 601 (2005)
35 M. Brack, R.K. Bhaduri, *Semiclassical Physics* (Frontiers Phys. **96**) (Addison-Wesley, Reading, MA, 1997)
36 B.D. Coleman, R.S. Falk, M. Moakher, Physica D **89**, 123 (1995)
37 J. Eggers, Phys. Rev. Lett. **80**, 2634 (1998)
38 A.J. Bernoff, A.L. Bertozzi, T.P. Witelski, J. Statist. Phys. **93**, 725 (1998)
39 J. Bürki, Adv. Sci. Technol. **44**, 185 (2004)
40 D.F. Urban, H. Grabert, Phys. Rev. Lett. **91**, 256 803 (2003)
41 D.F. Urban, J. Bürki, A.I. Yanson, I.K. Yanson, C.A. Stafford, J. van Ruitenbeek, H. Grabert, Solid State Commun. **131**, 609 (2004)
42 R.S. Maier, D.L. Stein, Phys. Rev. E **48**, 931 (1993)
43 P.Z. Coura, S.B. Legoas, A.S. Moreira, F. Sato, V. Rodrigues, S.O. Dantas, D. Ugarte, D.S. Galvão, Nano Lett. **4**, 1187 (2004)